

## Investigation of stability characteristics of cold-season convective precipitation events by utilizing the growth rate parameter

Christopher J. Melick,<sup>1</sup> Patrick S. Market,<sup>1</sup> Larry L. Smith,<sup>1,2</sup> Brian P. Pettegrew,<sup>1</sup> Amy E. Becker,<sup>1</sup> and Anthony R. Lupo<sup>1</sup>

Received 12 June 2007; revised 11 September 2007; accepted 19 December 2007; published 22 April 2008.

[1] The seldom utilized growth rate parameter ( $\sigma^2$ ), which predicts how rapidly a small-amplitude disturbance will grow in a conditional symmetrically unstable environment, was applied to study the stability characteristics of convective precipitation case studies across the central United States during the winter seasons of 2003–2004 and 2004–2005. The goals were to improve our understanding of how the environment becomes destabilized over a relatively short period of time, as well as to determine approximately where and when elevated thunderstorms are likely to develop. The comprehensive evaluation comprised a case study example and summary of statistics obtained by tabulations at the initiation site and spatial compositing of all case studies identified. The doubling time for the convection (the time required for a convective element to achieve twice its current depth) was found to be on the order of 1.3 h, which is consistent with the typical timescale for moist slantwise convection resulting from the release of conditional symmetric instability. The development of cold-season precipitation with lightning (i.e., thundersnow) and any associated banding was correctly and most accurately predicted from trends in plots of  $\sigma^2$  analyzed at the level at which the highest significant growth rates occurred. While this naturally varied from one event to the next, the average elevation tended to be close to 650 hPa. Furthermore, a term-by-term diagnosis of the mathematical expression for the growth rate was determined to be quite useful as another means of identifying the type of instability released within instances of wintertime convection. By calculating the individual contributions to the growth rate and observing whether a positive or negative response was obtained, the nature of the stability regime present was also ascertained. The inclusion of a set of non-thundering snowstorms helped to substantiate the assumption that atmospheres are less stable and more susceptible to vertical motions during those occasions where lightning develops in wintertime scenarios. Thus an outlook for elevated, cold-season thunderstorms can be more accurately issued by identifying regions where reduced values of equivalent potential vorticity (i.e., small symmetric stability or instability) are collocated with estimates of high  $\sigma^2$  (i.e., where small-scale slantwise perturbations will grow). Given the overall success, it is hoped that some of the conclusions established by this work will be implemented routinely in an operational environment and provide forecasters an additional, essential tool in dealing with nowcasting situations of hazardous winter weather events.

**Citation:** Melick, C. J., P. S. Market, L. L. Smith, B. P. Pettegrew, A. E. Becker, and A. R. Lupo (2008), Investigation of stability characteristics of cold-season convective precipitation events by utilizing the growth rate parameter, *J. Geophys. Res.*, *113*, D08108, doi:10.1029/2007JD009063.

### 1. Introduction

[2] Curran and Pearson [1971] were among the first to investigate the occurrence of snow with thunder (“thunder-

snow”) across the United States. Their study, along with others [e.g., Holle and Cortinas, 1998; Market *et al.*, 2002], indicated a tendency for such events to occur over specific geographical regions, the central United States being one of those preferred locations. Unlike the more easily identifiable surface influences, such as orographic and lake-effect processes [Schultz, 1999], many cases of convective snowfall have resulted from the release of elevated instability within the much larger circulation pattern of extratropical cyclones

<sup>1</sup>Department of Soil, Environmental and Atmospheric Sciences, University of Missouri-Columbia, Columbia, Missouri, USA.

<sup>2</sup>Currently at National Weather Service, Monterey, California, USA.

(ETC) [Market *et al.*, 2002]. Recent work has revealed a unique vertical thermodynamic profile for such elevated thundersnow events [Market *et al.*, 2006], where a mid-tropospheric layer of weak static stability ( $>6.5 \text{ K km}^{-1}$ ) exists above a frontal inversion. Additionally, Crowe *et al.* [2006] examined 30-years of thundersnow cases in the upper Midwest United States and found that most were associated with significant snow accumulations ( $>15 \text{ cm}$ ) within  $\approx 110 \text{ km}$ . Thundersnow events are thus more than a mere curiosity, but are often associated with heavy snowfall and a unique sounding signature that can signal its presence. Moreover, we know that the events examined were almost certainly convective in nature.

## 2. The Growth Rate Parameter

[3] Narrow lines of clouds and precipitation are often found in the vicinity of frontal systems. In order to explain the origin of these banded features, Bennetts and Hoskins [1979] revealed evidence through numerical modeling and observations that conditional symmetric instability (CSI) might be an important mechanism. After finding that the criterion for symmetric instability in a dry atmosphere was rarely satisfied, they considered the influence of moist processes on the flow regime within a two-dimensional, semigeostrophic framework. Results indicated that unstable, slanted roll circulations were more plausible if diabatic effects, such as latent heat release, were included. Thus the necessary “condition” for releasing CSI was that the environment had to be at or near saturation, with perturbations accelerating upward and laterally toward colder air if the displacement was between the geostrophic pseudo-angular momentum ( $M_g \equiv \vec{V}_g + f\hat{x}$ , where  $x$  is the distance along the cross-section taken perpendicular to the midtropospheric baroclinic zone) and the more steep wet-bulb potential temperature surfaces ( $\theta_w$ ) [e.g., Bennetts and Hoskins, 1979; Emanuel, 1983a, 1983b].

[4] In their work on growth rates of slantwise convection, Bennetts and Hoskins [1979] obtained a doubling time (the time required for a convective element to achieve twice its current depth) for CSI on the order of a couple of hours. By assuming very moist conditions and taking into account possible motions around a hypothetical “tube” of air, they were able to formulate an expression for  $\sigma^2$ :

$$\sigma^2 = -\frac{q_w}{N_w^2} = -\frac{\frac{f\vec{g}}{\theta_o}(\vartheta_g \cdot \nabla_3\theta_w)}{\frac{g}{\theta_o} \frac{\partial\theta_w}{\partial z}}, \quad (1)$$

which represented the ratio of the wet-bulb potential vorticity ( $q_w$ ) to the moist static stability ( $N_w^2$ ). In the above expression for equation (1),  $\theta_o$  represents a reference potential temperature (283 K [Bennetts and Sharp, 1982]),  $\vartheta_g$  the three-dimensional geostrophic absolute vorticity vector,  $\nabla_3$  the three-dimensional gradient vector in cartesian ( $x, y, z$ ) coordinates, and the remaining variables take on their usual meteorological meanings. The units of  $\sigma^2$  are inverse time (hours) squared, which will be expressed as  $\text{h}^{-2}$ , with positive (negative) values expected to indicate growth (decay) of a disturbance introduced into the prescribed environment.

[5] Bennetts and Sharp [1982] directly applied equation (1) to the relevance of CSI and the occurrence of mesoscale frontal rainbands and found that the growth rate parameter was more useful in the prediction of banded precipitation than in identifying occasions where the rainfall was uniform. In particular, the structure of any frontal precipitation was likely to be banded for  $\sigma^2 \geq 0.2 \text{ h}^{-2}$ , with banding less likely for lower values. In situations where small positive or negative growth rates were obtained, discrimination of banded from non-banded precipitation was difficult, as approximately half of the events fell into each category. Since there are multiple causes for banded precipitation, the presence of banded structures does not necessarily mean that the cause is associated with the release of CSI and/or the destabilization of the background atmospheric environment. Rather, the existence of such mesoscale features can be explained through several other dynamical theories [e.g., Parsons and Hobbs, 1983] which are not discussed in the current work. Thus caution will be observed when correlating elongated patterns in the radar reflectivity against regions of high  $\sigma^2$  values.

[6] In order to gain more instructive insight, equation (1) can be rewritten by expanding  $q_w$  into its vertical and horizontal components and utilizing the thermal wind relationship, as was done by Bennetts and Sharp [1982]. Upon converting from height to pressure coordinates and eliminating density through the equation of state, an alternative form for the development of small amplitude disturbances was obtained:

$$\sigma^2 = \underbrace{-f\eta_g}_{\text{(A)}} - \underbrace{\frac{RT}{p\theta_o} \frac{\nabla_h\theta \cdot \nabla_h\theta_w}{\frac{\partial\theta_w}{\partial p}}}_{\text{(B)}}, \quad (2)$$

where  $\eta_g$  represents the vertical component of the geostrophic absolute vorticity vector and  $\nabla_h$  is the horizontal gradient operator. An examination of equation (2) showed that several constituents contribute to the magnitude and sign of  $\sigma^2$ . By itself, a particular value for the growth rate parameter will not be able to identify type(s) of instability, let alone assure that any is present. Consequently, for this purpose, Bennetts and Sharp [1982] advocated that an evaluation of the individual terms in equation (2) as well as an analysis of the corresponding synoptic pattern be performed.

[7] Bennetts and Sharp [1982] noted that conditions favorable for the development of CSI occur in regions where the two right-hand-side terms in equation (2) are of similar magnitude. Still, atmospheres characterized by other types of instability can be associated with estimates provided by  $\sigma^2$ , despite whether positive or negative values are obtained. For instance, an inertially unstable environment exists in situations when term (A)  $\geq 0$  and when term (A)  $\gg$  term (B). Whereas term (A) is composed of just an inertial contribution ( $-f\eta_g$ ), term (B) is composed of three more elements. The first of these (hereafter referred to as term B1), given by  $\frac{RT}{p\theta_o}$ , represents thermal properties of the fluid since  $R, p$  (usually 700-hPa), and  $\theta_o$  are all constants. As for the second contribution (hereafter referred to as term B2),  $\nabla_h\theta \cdot \nabla_h\theta_w$  corresponds to the orientation of the potential temperature gradient with respect to the wet-

bulb potential temperature gradient. Alternatively, this is equivalent to the projection of one gradient onto the other, in which the term will have its maximum value when the two vectors are aligned. A result of zero, however, would result should one was perpendicular to the other. Furthermore, the dot product stipulates that a positive (negative) sign for this particular contribution can only be obtained when the gradients point in the same (opposite) direction, such as when relatively warm air is coincident with relatively moist (dry) air. The last of the elements (hereafter referred to as term B3) represents the moist static stability of the environment ( $\frac{\partial\theta_w}{\partial p}$ ) and generally plays an increasingly significant role in  $\sigma^2$  as the atmosphere becomes less convectively stable ( $\frac{\partial\theta_w}{\partial p} \rightarrow 0$ ). A positive value for  $\frac{\partial\theta_w}{\partial p}$  would signal the existence of convective instability sufficient for supporting vertical accelerations and upright convection, which will become the dominant mode due to its faster growth rate [Weismuller and Zubrick, 1998]. This is a condition outside the purview of  $\sigma^2$ . Rather, growth or decay of a disturbance will be determined ultimately by considering all contributing terms and their associated signs and magnitudes collectively within equation (2).

[8] One technique that has historically been advanced to determine the presence of instability in the atmosphere has been the identification of regions where the moist geostrophic potential vorticity ( $MPV_g$ ) is less than zero [Schultz and Schumacher, 1999; and references therein]. Many researchers [e.g., Emanuel, 1983a; Sanders and Bosart, 1985; Moore and Lambert, 1993; McCann, 1995; Nicosia and Grumm, 1999; Clark et al., 2002; Jurewicz and Evans, 2004; Moore et al., 2005] have employed a form known as the equivalent potential vorticity (EPV), and this study follows suit. Specifically, McCann [1995] recognized that the three dimensional vector representation of EPV ( $q_e \equiv -g\vartheta_g \cdot \nabla_3\theta_e$ ) can be simplified by neglecting the vertical velocity terms and Coriolis term in the along-shear direction; by applying these approximations and carrying out the dot product, McCann [1995] obtained:

$$q_e = g \left( \frac{\partial\theta_e}{\partial x} \frac{\partial v_g}{\partial p} - \frac{\partial\theta_e}{\partial y} \frac{\partial u_g}{\partial p} - \left( \frac{\partial v_g}{\partial x} - \frac{\partial u_g}{\partial y} + f \right) \frac{\partial\theta_e}{\partial p} \right), \quad (3)$$

wherein computations can be easily obtained from gridded output of numerical weather models. Negative values of EPV, in themselves, are necessary but not sufficient for convection to develop. Rather, the ingredients based methodology [Johns and Doswell, 1992; Schultz and Schumacher, 1999] also requires both a forcing mechanism to lift air parcels as well as ample amounts of moisture for the release of either CI or CSI to occur.  $\sigma^2$  is then used to assess the rate of growth of a disturbance in that environment.

### 3. Methodology

#### 3.1. Selection of Thundersnow Cases

[9] Surface observations from weather stations across the United States were scanned routinely during the winter months (October–April) of 2003–2004 and 2004–2005. In order to document the occurrence of thundersnow during this time period, reports of thunder with various intensities

of snowfall were counted, such that the lightning was either observed near the surface station or at some distance away. From this data set, only events associated with an extratropical cyclone (ETC) occurring in the region between the Rocky and Appalachian Mountain ranges (i.e., the central part of the country) were investigated further. Following the methodology applied by Market et al. [2002], twenty-nine separate case studies with corresponding initiation sites were identified by employing an appropriate temporal and spatial criterion for mesoscale processes. Specifically, the identification of distinct events was accomplished by checking whether either of the two following conditions was met: the separation distance at different stations for simultaneous thundersnow reports had to be more than 1100 km or more than 6 h had to pass with consecutive reports at the same station. This procedure was selected by Market et al. [2002] as a reasonable means of discriminating TSSN episodes given the sufficiently unique characteristics of the individual flow regimes.

[10] In order to further substantiate the existence of thundersnow in these case studies, cloud-to-ground (CG) lightning flash data were obtained from the National Lightning Detection Network (NLDN). While a large portion of the lightning that results from cold season, elevated convection is intracloud, Smith et al. [2005] utilized the NLDN as a means to provide additional, solid evidence that lightning activity occurred within half of the archived snowstorms from the 2003–2004 season. Furthermore, a more accurate identification of initiation was determined at times by plotting CG-lightning flashes from the NLDN in conjunction with surface weather conditions from nearby surface observations, despite that fact that a report of thundersnow was lacking from the individual observations. It is worth noting that the change-over to automated observing stations in the mid-1990s made thundersnow observations less reliable and likely reduced the detection rate. The current methodology helped to obtain additional precision in determining the location and onset of convective snowfall, something which Smith et al. [2005] emphasized would be important to operational forecasters and their capacity to notify the general public in a timely manner of approaching hazardous weather. By applying this evaluation scheme to the current work, results from this examination were restricted to the seventeen selected thundersnow cases given in Table 1, these being episodes where lightning flashes could be verified from the NLDN (one event was left out due to the relatively low amount of moisture present in the sounding profile since the growth rates would require near-saturated conditions).

#### 3.2. Analysis Routine

[11] Each of the right-hand-side terms in equations (2) and (3) were calculated utilizing the GENERAL Meteorological PAcKage (GEMPAK) [desJardins et al., 1991] software, with the initial analysis from a 40-km Rapid Update Cycle (RUC-2) model grid providing the necessary input data. Calculations were performed every 50-hPa in the model from 950-hPa to 550-hPa and second-order finite differencing was utilized to evaluate vertical derivatives. This approach produced some noise in the analyses, as expected [Barnes et al., 1996]. Comparison to results from a filtered, 80-km RUC file from the same time produced

**Table 1.** Information on Subset of Convective Snow Case Studies Examined<sup>a</sup>

Location of TSSN Onset	Onset Time	LHSGR(hPa) (Onset, Prior)
Salina, Kansas (KSLN)	03/11/23 0400	(700, 800)
Beatrice, Nebraska (KBIE)	03/12/09 1500	(600, 700)
Tulsa, Oklahoma (KRVS)	03/12/10 0400	(600, 800)
Marion, Illinois (KMWA)	04/01/27 0400	(750, None)
Mountain Home, Arkansas (KBPK)	04/02/05 0300	(550, 600)
Near Eau Claire, Wisconsin (44.6N;90.9W)	04/03/05 0700	(550, 650)
Hutchinson, Minnesota (KHCD)	04/03/13 1300	(700, 550)
Amarillo, Texas (KAMA)	04/11/02 0900	(550, 600)
Kansas City, Missouri (KMKC)	04/11/24 0700	(650, 700)
Cape Girardeau, Missouri (KCGI)	04/12/22 0900	(600, 550)
Owensboro/Davies, Kentucky (KOWB)	04/12/23 0200	(800, 800)
Near Watertown, South Dakota (45.1N; 96.9W)	05/01/01 1600	(700, 600)
Near Terre Haute, Indiana (39.88N; 87.26W)	05/01/08 0600	(550, 550)
Lincoln, Illinois (KAAA)	05/01/22 0800	(650, 750)
Benton Harbor, Michigan (KBEH)	05/02/20 1700	(600, 800)
Near Albert Lea, Minnesota (43.5N; 92.45W)	05/03/18 1100	(550, 550)
Goodland, Kansas (KGLD)	05/04/11 0400	(700, 750)

<sup>a</sup>Location of thundersnow onset is given along with surface weather station identifier when possible. Onset time indicates year, month, date, and closest hour (UTC) for which the first report occurred. As described in the text, the level with the highest significant growth rates [LHSGR(hPa)] is determined for each event at initiation as well as 3-hours prior.

nearly identical (although smoother) patterns. Still, application of the geostrophic wind at such a fine resolution is most likely not appropriate. Thus a simple Gaussian filter was applied to significantly damp artificial structures at the shortest wavelengths in the raw fields while still retaining true small-scale features. The degree of filtering chosen acted to substantially decrease wave amplitude for length scales below 240-km, thereby mostly eliminating information that would be considered noise in an atmosphere that is in approximate geostrophic balance.

[12] The RUC-2 numerical model [Benjamin et al., 1998] is unique in its frequent hourly assimilation of the most recent observations, thus providing high-quality analyses and short-range forecasts [Benjamin et al., 2004a, 2004b]. This advantage is important in examining and noting short-term trends in stability characteristics of thundersnow events, especially considering that such phenomena have horizontal dimensions in the meso- $\beta$  scale range and typically exhibit a timescale on the order of just a few hours [e.g., Emanuel, 1986; Market et al., 2002]. Moreover, Curran and Pearson [1971] noted that traditional indices would often not produce accurate estimates of instability at the time of the proximity sounding given the fact that convection has already begun. As a result, this study not only investigates the time of initiation, but also takes into account preconditioning of the environment three hours beforehand.

[13] In order to remain consistent with Bennetts and Sharp [1982], calculations of  $\sigma^2$  were initially performed at 700-hPa and considered significant only in regions where the relative humidity (RH) exceeded 80%. This latter criterion was applied to ensure sufficient moisture in the atmosphere, a necessary condition, as mentioned earlier, in diagnosing the presence of CI or CSI. Indeed, a standard RH of 80% represents a saturated condition with respect to

ice for temperatures that support dendrite growth ( $-13^{\circ}\text{C}$  to  $-18^{\circ}\text{C}$ ). However, given the natural variability in synoptic conditions which exist from one case study to the next, evaluating the likelihood of wintertime convection from one set pressure level is not the best approach. For this reason, an alternative technique was pursued by obtaining separate estimates of  $\sigma^2$  at the level with the highest significant growth rates (LHSGR) present, which ordinarily was different than 700-hPa. In this way, the authors believe that a more plausible measure of the source and nature of elevated thunderstorms would generally be obtained at the elevation experiencing the least resistance to slantwise perturbations. One of the criteria for the LHSGR was that the assessment did not begin until above 850-hPa in order to make certain that the analysis was above ground level as well as avoid spurious results near the surface. The use of the word significant in the acronym was the final crucial factor and again meant that ample moisture had to be present for the parcel instability to be realized. The pressure level for the LHSGR three hours before and at the time of initiation is documented in Table 1.

### 3.3. Snowband Classification Scheme

[14] A subjective set of criteria were used to classify snowbands. The development of most synoptic-scale and embedded mesoscale precipitation structures is often related to the evolution of airstreams within ETCs. While this observation has been known implicitly since the days of the Norwegian Cyclone Model (NCM) developed by Bjerknes and Solberg [1922], the explicit representation of three main conveyor belts and their associated interactions is more recent [e.g., Carlson, 1980]. Within the extensive zone of weaker ascent in the warm conveyor belt (WCB), enhanced and constricted updrafts are often contained over regions spanning tens to a few hundred kilometers wide. Intense precipitation from these larger mesoscale areas tend to take on structures sufficiently elongated that an orientation can be assigned. Frequently referred to as bands, the length to width ratio are defined to be at the very least 2:1 [e.g., Houze et al., 1976; Hane, 1986; Byrd, 1989; Browning, 1990; Novak et al., 2004]. Furthermore, Wallace and Hobbs [1977] cited typical horizontal areas covered by these banded features to be on the order of  $10^3$ – $10^4$  km<sup>2</sup>. Although common lifetimes for such events are noted to be on the order of hours, the exact duration tended to be less restrictive in some observational work [e.g., Byrd, 1989] than in others [e.g., Bennetts and Sharp, 1982; Novak et al., 2004]. Furthermore, Browning [1990] also indicated that the wide mesoscale precipitation bands generally have an orientation parallel to the vertical wind shear within the middle troposphere, with any embedded convection often developing above the more stable surface layer. Still, within the context of being able to identify a moving reflectivity pattern for a set period of time, no widely accepted lower limit is present in the literature. Consequently, because of these varying degrees of ambiguity, a subjective criteria method for banded precipitation was formulated.

[15] The resultant classification scheme deals strictly with defining cold-season precipitation band areas without reference to the type or number present (single or multiple). The comparisons of individual observed radar features against the theoretical fields generated by the mesoscale model do

**Table 2.** Information on Subset of Non-Thundering Snow Case Studies Examined<sup>a</sup>

Non-TSSN Location	Midpoint Time	LHSGR(hPa) (Midpoint, Prior)
Green Bay, WI (KGRB)	02/04/02 1200	(700, 600)
Springfield, MO (KSGF)	03/01/16 1200	(750, 800)
Omaha/Eppley, NE (KOMA)	03/02/15 1200	(700, 700)
Omaha/Eppley, NE (KOMA)	04/03/15 1200	(550, 550)
Green Bay, WI (KGRB)	05/01/06 1200	(650, 550)
Green Bay, WI (KGRB)	05/01/22 1200	(800, 650)
Green Bay, WI (KGRB)	05/02/14 1200	(550, 800)

<sup>a</sup>The time given is year, month, date, and hour of the midevent period. The location is distinguished by station identifier. Similar to Table 1, the LHSGR(hPa) is determined for each event at the midpoint as well as 3-h prior.

not always reveal correspondence between one another, the amount of variation particularly dependent upon differences in the resolution. Like the case study of heavy banded snowfall by *Martin* [1998], the current work also employed a grid point spacing of 40-km which is too coarse to explicitly represent CSI circulations (let alone those caused by CI). However, like *Martin*, the authors were only interested in evaluating those regions of the atmosphere wide enough to be identifiable in model output and meet the necessary conditions for elevated instability and destabilization. In other words, the desired goal was to examine whether there was general agreement in the patterns in reflectivity data and major areas of precipitation with those of  $\sigma^2$ , as advanced by *Bennetts and Sharp* [1982]. Consequently, it was expected that the finer details would not be captured, such as multiple bands being present within a broad region of positive growth rates. As a result, the criteria were that the bands be greater than 200-km in length, possess a width of approximately 50 to 100-km, and have coherent structures with a minimum intensity of 25 dBZ maintained throughout a majority of their length for at least an hour. These standards are comparable to the transitory banded category of *Novak et al.* [2004] and the banded (B) or weakly banded (WB) categories defined by *Byrd* [1989]. The constraint of consistent movement throughout the entire evolution by *Bennetts and Sharp* [1982] will be applied in instances where the midtropospheric mean flow is aligned with the band of precipitation, something which could realistically occur northwest of a surface cyclone.

### 3.4. Selection of Non-Thundering Snowstorm Cases

[16] The combination of surface observations and the NLDN allowed the ability to select snowstorms associated with an ETC but without the presence of lightning. The process, established by *Smith* [2006] and *Market et al.* [2006], is similar in many respects to determining episodes of thundersnow. The idea was to diminish both orographic and lake-effect influences by restricting the domain to the same interior portion of the country and picking cases that had snowfall accumulations and rates comparable to the convective snow subset in the climatology of *Market et al.* [2006]. More precisely, observed visibility had to be less than or equal to  $\frac{1}{4}$  statute mile for an extended time frame, such that the midpoint was defined as the time of balloon flight (1200/0000 UTC). Besides the detection of CG flashes from the NLDN, the absence of lightning was

further bolstered by the fact that human observers were frequently present at the station locations given in Table 2. For the purpose of the current work, the identical set of non-thundersnow (non-TSSN) events used by *Smith* [2006] was evaluated. So as to keep differences between TSSN and non-TSSN limited to just physical mechanisms in the atmosphere, the analysis routine is kept consistent. The RUC-2 is relied upon once again for computations and synopses, with the acquisition of results from some of the techniques previously explained also explored. Following the format established in Table 1, seven non-TSSN events (encompassing four winter seasons from 2002-2005) are listed in Table 2.

### 3.5. Point Value Statistics and Composites

[17] The examination of  $\sigma^2$  and 3-D EPV were pursued in two different fashions. The first was more quantitative and entail compiling averages and standard deviations for point values in each case study. To be more precise, these statistics were derived from the individual initiation (TSSN) or midpoint (non-TSSN) sites and provided some idea of the expected sign and magnitude for the metrics diagnosed at the place of interest. Since each station identifier or pair of latitude and longitude coordinates demarked a specific position not exactly matching the grid points in the RUC-2 model, significance of the results was limited to some extent by the utilization of bilinear interpolation. Furthermore, while some effort has been devoted to show that statistical significance has been achieved for some stability indices [e.g., *Market et al.*, 2006], the precision needed for anticipating activity at specific point locations was generally unattainable. Rather, some practical benefit could be attained by using pattern recognition.

[18] Plots of atmospheric properties, whether they were directly observed or indirectly derived, were also pursued and helped to complement the tabular results already established. Instead of inspecting each case study individually for this objective, discrete spatial composites were produced for both TSSN and non-TSSN situations through means of a moving grid. The size of the subdomain ( $31 \times 31$  grid points) in this study was sufficiently large (1200 km) to capture the background (meso- $\alpha$  to synoptic-scale) aspects associated with both types of snowstorms. Seeing that the origin in the spatial framework has been known to track many analyzed meteorological phenomenon [e.g., *Mote et al.*, 1997; *Moore et al.*, 2003; *Oravetz*, 2003], the scheme here established two separate storm-relative composites by centering on the initiation sites of TSSN (Table 1) in one and the midpoint locations for non-TSSN (Table 2) in the other, where the *nearest* grid point in the RUC-2 model represented the centroid. It should be stressed that the calculation of  $\sigma^2$  and other expressions discussed in the text occurred before compositing for the strict intention to avoid additional, artificial smoothing in creating averaged and standard deviation fields.

## 4. Results

### 4.1. General Results From the 2003–2004 and 2004–2005 Winter Seasons

[19] Reflectivity data with the best resolution available (most often 1 km; obtained from <http://hurricane.ncdc>.

**Table 3.** The Counts of Banded and Non-Banded Occurrence are Binned According to Value Ranges in the Filtered Growth Rate Parameter ( $\sigma^2$ ;  $\text{h}^{-2}$ ) Calculated From the RUC-2 Model<sup>a</sup>

A.	Predicted Non-Banded			Predicted Banded	
	<-0.1	-0.1 to 0	0.01 to 0.1	0.11 to 0.19	$\geq 0.2$
700-hPa $\sigma^2$					
Non-banded observed	8	3	0	0	1
Banded observed	1	0	1	0	3
B.	Predicted Non-Banded			Predicted Banded	
	<-0.1	-0.1 to 0	0.01 to 0.1	0.11 to 0.19	$\geq 0.2$
LHSGR $\sigma^2$					
Non-banded observed	1	4	3	1	3
Banded observed	0	0	0	0	5

<sup>a</sup>This is accomplished at thundersnow onset location and time period and performed at both (A.) 700-hPa and (B.) the LHSGR(hPa). When comparing against the observational evidence in each case study, the existence of mesoscale banded areas of precipitation near time of initiation is determined from the classification scheme described in the text.

noaa.gov/pls/plhas/has.dsselect) were examined from WSR-88D radar stations in each of the thundersnow events listed in Table 1. Only the 5 March 2004 case study presented a scenario where no suitably close level II radar data were available, so the more coarse 6 km level III composite information was evaluated instead utilizing GEMPAK. Table 3 provides a diagnosis of mesoscale banding from the observational evidence, and also presents corresponding results for  $\sigma^2$  (conventional as well as from the level of highest significant growth rates [LHSGR]). Besides the point values given for the initiation sites, plan view analyses of the growth rate parameter complemented the profile information and provided a more complete 3-D evaluation of the atmosphere leading up to the onset of convective snowfall. With respect to the horizontal plots, graphical examples of the RUC-2 model output will be provided later when the individual case study is presented.

[20] An initial inspection of the tendencies from  $\sigma^2$  reveals considerable variations in both sign and magnitude from one episode to another, especially for the numerous nonbanded events observed (Table 3). The progression and sometimes intensification of already robust radar reflectivity returns (usually  $>30$  dBZ) into the area of interest corroborated the nowcast that wintertime convection might transpire in the near future. This increase in intensity is further supported by the upward trend in average values for  $\sigma^2$  compiled in Table 4, when comparing the value at the time the event commenced to that from three hours prior, regardless of whether the conventional method advocated by *Bennetts and Sharp* [1982] or the application of the LHSGR was applied. However, more favorable results were obtained with higher  $\sigma^2$  values for both time periods at the LHSGR (compare Tables 4A to 4B), which was typically close to the 650-hPa level. More support for this conclusion was reached by computations of 3-D EPV [McCann, 1995], the statistical results of which are also shown in Table 4. Although a substantial number of the thundersnow cases exhibited evidence of weak stability to instability within the vertical profiles, the averages and large standard deviations

for EPV showed that values varied substantially (Table 4). Again, results from this metric revealed that less opposition (i.e., slightly positive to negative estimates) to elevated thunderstorm development was offered at the LHSGR. Along these lines, average values for  $\sigma^2$  at the time of initiation increased from  $-0.01 \text{ h}^{-2}$  to  $0.30 \text{ h}^{-2}$  (see Table 4B) when the more novel approach was used. This latter value corresponds to a  $\sigma$  equal to  $0.55 \text{ h}^{-1}$  or a doubling time for the disturbance every 1.3 h, which is approximately consistent with the established timescale ( $f^{-1}$ ) for moist slantwise convection generated from the release of CSI [e.g., *Bennetts and Hoskins*, 1979; *Emanuel*, 1986].

[21] Five of the seventeen thundersnow events examined at the time of initiation met the criteria for banded structures developed for the current work (Table 3). While the width was typically on the order of 50-km, lengths varied from 200 to 700-km and the precipitation bands lasted for periods of 1 to 3 h. Reflectivity magnitudes within the colder area of precipitation generally ranged from 25–40 dBZ, with much higher values occurring in a few instances. However, in these rare occurrences, the presence of a strong elevated warm nose in RUC-2 soundings and thickness (the depth of a layer bounded by two isobaric surfaces) analyses indicated that some of the precipitation reaching the surface was probably of the mixed variety. For all five banded precipitation areas identified in the observations, the evaluation of horizontal, 2D plots and vertical profiles of  $\sigma^2$  compared well in each instance. In this regard, Table 3 also reveals that more favorable results were again obtained by selecting the LHSGR, where the stability tendencies more easily surpassed the  $0.2 \text{ h}^{-2}$  criterion. In fact, at this particular level, all of the observed instances of precipitation banding were associated with growth rates greater than this value.

[22] However, high values of the growth rate parameter are not a sufficient condition for banded precipitation. From this particular vantage point, banded precipitation areas were expected to occur in eight convective snow events (Table 3) as the growth rates were sufficiently high, positive values although only five were predicted correctly. Alternatively, the potential for amplification of small parcel perturbations in the midlevels of the atmosphere could also be observed by the fact that negative LHSGR EPV estimates occurred in this specific subset of events (not shown).

**Table 4.** Average and Standard Deviation [ $\mu$  ( $s$ )] Values of Filtered Equivalent Potential Vorticity (EPV;  $10^{-6} \text{ K kg}^{-1} \text{ m}^2 \text{ s}^{-1}$ ) and Growth Rate Parameter ( $\sigma^2$ ;  $\text{h}^{-2}$ ) for All Events Listed in Table 1<sup>a</sup>

(A) 700-hPa	Initiation	Prior
$\sigma^2$	0.01 (0.33)	-0.43 (1.16)
3-D EPV	0.46 (0.77)	0.25 (0.49)
(B) LHSGR(hPa)	Initiation	Prior
$\sigma^2$	0.30 (0.59)	-0.01 (0.12)
3-D EPV	-0.03 (0.25)	0.26 (0.65)

<sup>a</sup>Values were calculated from the RUC-2 model and valid at thundersnow onset location and time period, with calculations performed at (A) 700-hPa and the (B) LHSGR(hPa). Results are also provided for 3-h prior to convective initiation. Since the atmosphere needed to be nearly saturated, statistical evaluation does not include those case studies in which the RH  $<80\%$ .

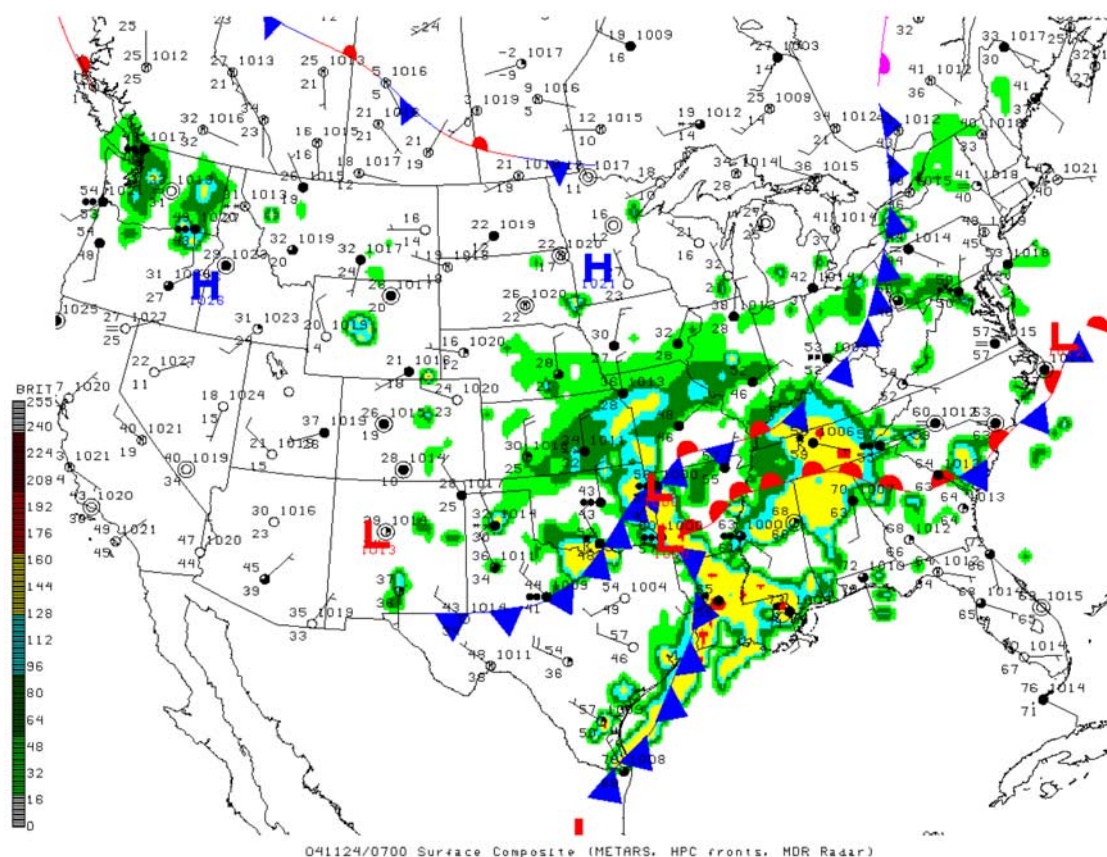


**Figure 1.** Surface composite (METARs, HPC fronts, and MDR radar reflectivity) valid at 0700 UTC 24 November 2004.

Consultation of the reflectivity pattern showed that banded structures did not occur in nearly half of the eight cases where the growth rate was large, with three time periods failing to meet the standards required in the classification scheme. Yet even with these particular exceptions, the radar analysis indicated that the convection more typically was organized as discrete cells, something which the RUC-2 model fields corroborated fairly well as the regions of higher value growth rates tended to be more circular in shape. Thus individual grid point values should not be the sole source of predicting the type of precipitation structure to expect. Rather, a more comprehensive assessment is offered by analyzing the distribution and arrangement of  $\sigma^2$  features made possible with horizontal charts. In order to graphically represent this particular advantage, figures will be provided for the case study presented. Finally, accuracy in anticipating nonbanded snowfall was dependent upon how the evaluation was accomplished. If the growth rates are analyzed at 700-hPa (Table 3a), values less than zero for  $\sigma^2$  captured all but one occurrence. By progressing vertically to the LHSGR (Table 3b), however, a much wider range of results are present for these 12 events. The one encouraging sign was that both approaches showed the probability of banding decreased as a function of decreasing growth rate. While the current sample size is too small to allow firm conclusions to be drawn for the general findings, the data tends to confirm the results of *Bennetts and Sharp* [1982].

## 4.2. Case Study (24 November 2004)

### 4.2.1. Synopsis: Surface, Upper-Air, and Radar Analysis

[23] The case study focuses on the first major winter weather system of the 2004–2005 season in the central part of the United States, which produced several inches of snow in the midst of substantial lightning activity. From the synoptic setup, the analysis in Figure 1 shows a 1000-hPa surface cyclone situated in northern Arkansas at 0700 UTC 24 November 2004, with the conventional observations suggesting air masses of remarkably different characteristics existing in close proximity. While a large region of precipitation was occurring on either side of the suitably analyzed frontal zones, conditions were only sufficiently cold for the frozen variety to accumulate north and west of the low-pressure center. Lightning was first detected in an area of snow near Kansas City, Missouri (KMKC; Figure 2) within the elongated axis of enhanced radar reflectivities oriented southwest to northeast across eastern Kansas and western Missouri. Temperatures were slightly above freezing (1–2°C range) in the vicinity of the surface stations where several CG flashes were present.

[24] Standard upper air charts of measured or easily derived variables (e.g., heights,  $\theta_e$ , geostrophic winds, absolute vorticity, and temperature advection) are presented at 0700 UTC in Figure 3. Panels (a), (b), (c), (d) correspond respectively to the 900-hPa, 700-hPa, 500-hPa, and 300-hPa

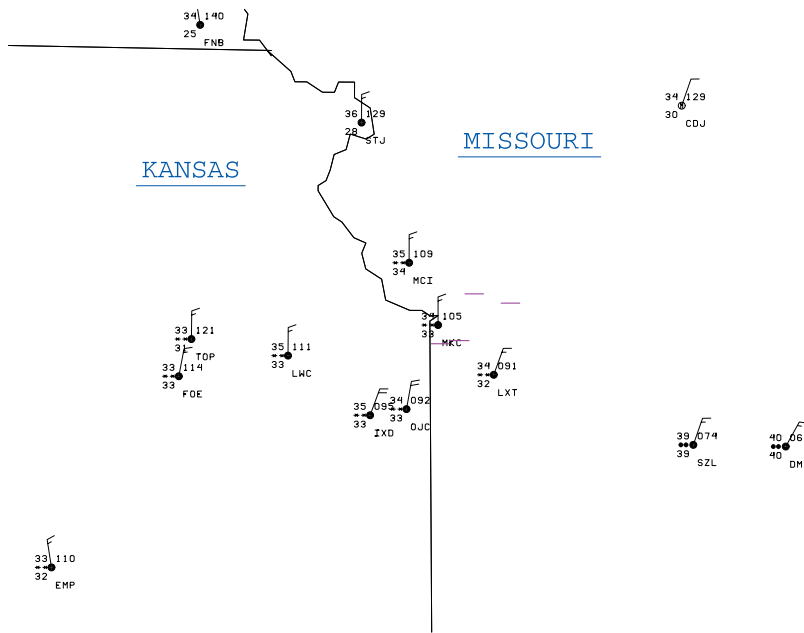


**Figure 2.** Standard plotted METAR observations valid at 0700 UTC 24 November 2004. The National Lightning Detection Network (NLDN) analysis of cloud-to-ground lightning strikes valid at 0710 UTC 24 November 2004.

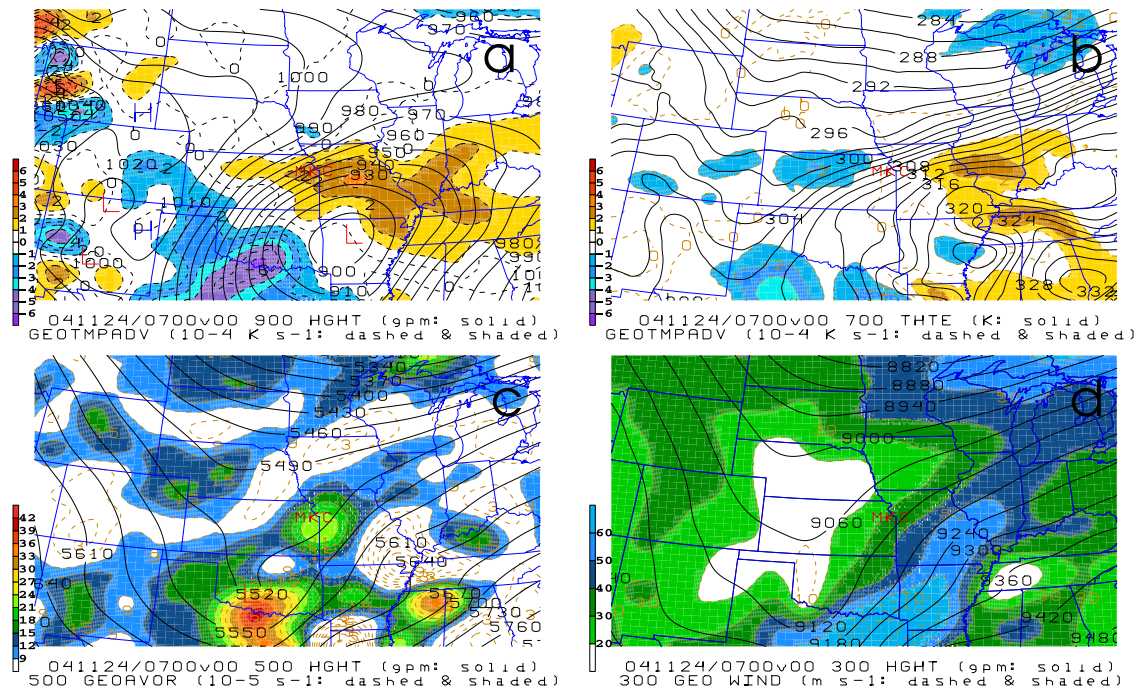


**Figure 3.** Standard upper air charts valid at 0700 UTC 24 November 2004 from the initial analysis of the 40-km RUC model. Panel (a) corresponds to 900-hPa height (gpm, solid lines) and geostrophic temperature advection ( $10^{-4} \text{ K s}^{-1}$ , dashed lines and color shading). Panel (b) corresponds to 700-hPa equivalent potential temperature ( $\theta_e$ ; K, solid lines) and geostrophic temperature advection ( $10^{-4} \text{ K s}^{-1}$ , dashed lines and color shading). Panel (c) corresponds to 500-hPa height (gpm, solid lines) and geostrophic absolute vorticity ( $10^{-5} \text{ s}^{-1}$ , dashed lines and color shading). Panel (d) corresponds to 300-hPa height (gpm, solid lines) and geostrophic isotachs ( $\text{m s}^{-1}$ , dashed and color shading). Location of initiation site is represented by surface station identifier MKC (Kansas City, MO).

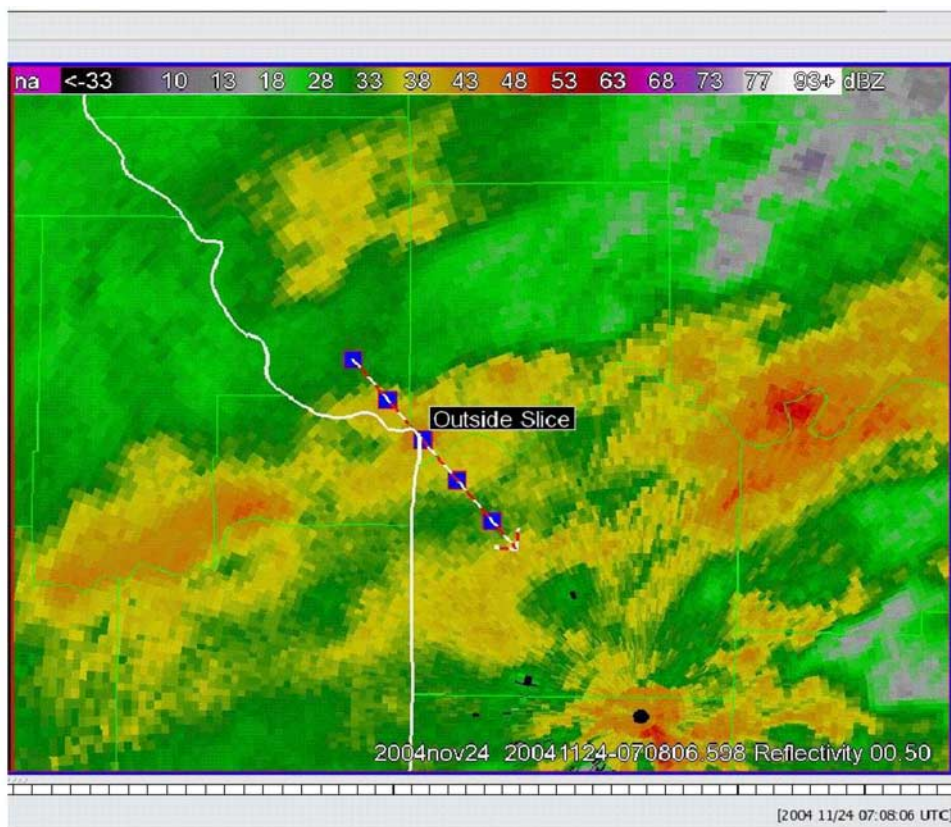


**Figure 4.** The radar reflectivity pattern ( $0.5^\circ$  tilt) displayed via WDSS and valid at 0708 UTC 24 November 2004 from the WSR-88D EAX radar site.

pressure levels, this selection following the average fields constructed for thundersnow events by *Market et al.* [2004]. The rationale was to identify the specific forcing mechanisms responsible for producing winter precipitation. Many of the basic synoptic features observed in this case study were present in the composites for convective snow occurring northwest of a surface cyclone (compare Figure 3 to Figure 1 by *Market et al.* [2004]). The warm air advection at 900-hPa was strongest just poleward of an intense closed low and near the initiation site (Figure 3a) and decreased in magnitude with height (Figure 3b). The 700-hPa analysis also shows a subtle  $\theta_e$  ridge extending up from the warm sector and wrapping around on the backside of the low level system from west to east in southern Missouri. Given the development of the trowal and the slight negative tilt in the 500-hPa (Figure 3c) and 300-hPa (Figure 3d) troughs, occlusion may be underway by the time of initiation. Furthermore, middle tropospheric positive vorticity advection and the left exit region of the jet streak were positioned near the area of interest. All of these thermodynamic and dynamic features imply an atmosphere suited for substantial upward vertical motions. The difference in details in the upper air analyses between this specific case and in a typical thundersnow event is to be expected as there is a natural loss of information which occurs in the compositing process. Nevertheless, as was intended by *Market et al.* [2004], pattern comparisons and recognition reveals that the similarities were noticeable.

[25] The more detailed search of banded features from data at the nearby WSR-88D site at Pleasant Hill, Missouri, revealed more such features near the beginning of this event (Figure 4). The narrow area of mixed precipitation lasted a couple of hours and was defined by a maximum length of 400-km and width of 50-km in the reflectivities often exceeding 30 dBZ. These qualifications met the designed classification scheme for this paper. However, this band was close to stationary during its lifetime due to the background flow in the middle troposphere being nearly parallel to the band and unable to effectively advect the disturbance (e.g., see Figure 5). A cross-section of the radar analysis was taken across the embedded convective cell over KMKC; while not overly impressive in terms of intensity and depth of the strongest reflectivities, a confined horizontal area of relatively higher returns from the radar extended upward a few kilometers from the surface (not shown).

#### 4.2.2. Growth Rates and Type of Instability

[26] The findings for  $\sigma^2$  in this case study were consistent with previous studies [*Bennetts and Hoskins, 1979; Bennetts and Sharp, 1982*] in accurately anticipating elevated convection, the type of storm structure, and identifying the source of the instability released in the background environment. A plot of the growth rates three hours prior to initiation (Figure 6a) shows the highest values south of the region of interest. This pattern matched up reasonably well with the intense activity from the radar occurring in approximately the same locale. As this area of elevated

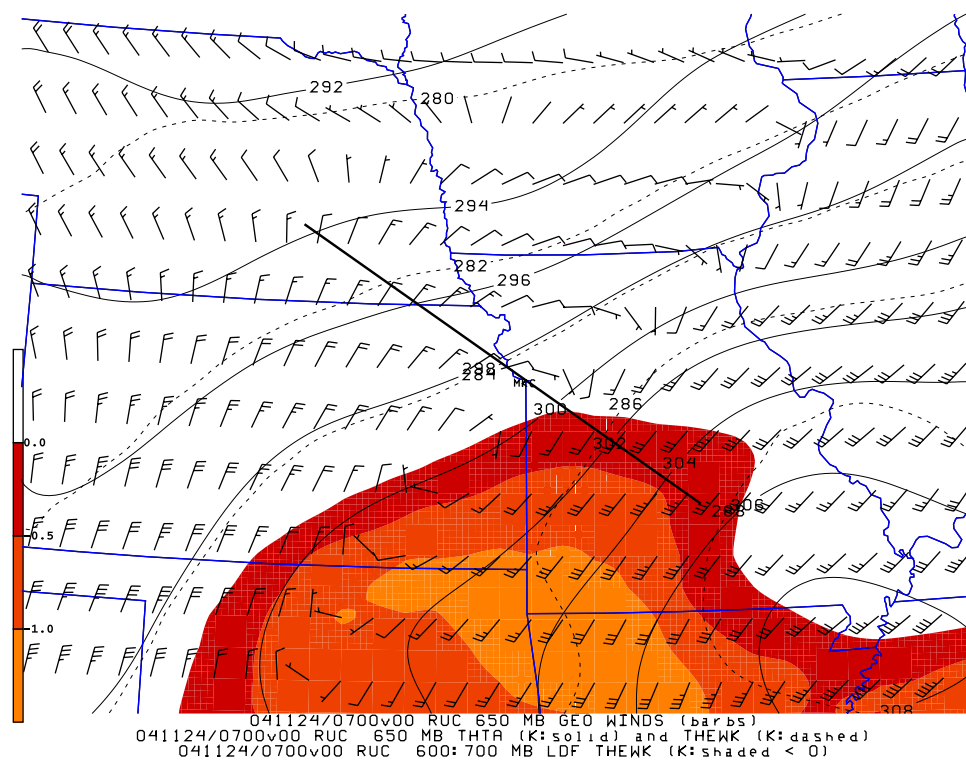


**Figure 5.** Same as in Figure 3 except for 650-hPa geostrophic wind barbs, potential temperature ( $\theta$ ; K, solid lines), wet-bulb potential temperature ( $\theta_w$ ; K, dashed lines), and 600–700 hPa layer difference wet-bulb potential temperature (K, color shading  $< 0$ ). Bold line denotes cross-section line in Figures 7, 8, and 9.

magnitudes progressed northward by 0700 UTC, the RUC-2 analysis at the LHSGR (650-hPa; Figure 6c) had the  $0.2 \text{ h}^{-2}$  zone (shaded) slightly more poleward and the pattern of  $\sigma^2$  near KMKC taking on more of a banded configuration compared to the RUC-2 analysis at the traditional 700-hPa level (Figure 6b). In this regard, the banding pattern in the radar reflectivities more closely corresponded to the area identified by the more novel approach of finding the level at which the growth rates maximized, with this altitude not always fixed from one event to the next (compare Figure 6 with Figures 1 and 4). Thus this prognostic appeared to be reliable in identifying spatial extent and determining expected movement of possible convective development.

[27] The presence of both low EPV values (small positive to negative) and high relative humidity in the analyses (Figure 6) reveals a moisture rich environment and instability over a sizable region of northwestern Missouri and southeastern Kansas, where temperatures were low enough for frozen precipitation to occur. While all of the essential ingredients were in place for convection to develop, the addition of the growth rate parameter in Figure 6 offered a means to refine the forecast area. The downward trend in stability (positive values of  $\sigma^2$ ) occurring in an atmosphere already prone to vertical/slantwise displacements of air parcels suggests that the most likely area for vigorous updrafts sufficient to produce lightning in the near future to be around the Kansas City area. Indeed, 11 CG flashes were recorded just in this area in a 35 minute time interval during the 0700 UTC hour on the 24th of November (not shown). The approach of combining several factors on a map to fine tune an area of concern is often followed during

the spring and early summer when severe weather is a concern over the central United States. While thunderstorms and their attendant precipitation are generally less frequent in the wintertime, many including *Schultz and Schumacher* [1999] and *Wetzel and Martin* [2001] advocate using an ingredients methodology to diagnose and predict their existence. Although substantial dynamics and moisture must be present in such situations [e.g., *Johns and Doswell*, 1992; *Schultz and Schumacher*, 1999], the stability of vertical or slantwise perturbations is often the discriminator in determining the potential for enhanced snowfall rates from convection [e.g., *Market et al.*, 2006]. Thus growth rates could be superimposed on top of EPV to facilitate the process of estimating the likely location and timing of heaviest snowfall.

[28] Equation (2) was partitioned into its individual terms in order to determine the type of stability regime present for this case study of thundersnow. The positive response for the growth rate was greater than  $0.2 \text{ h}^{-2}$ , a result arising because the total contributions from (B) adequately exceeded those from (A). The initiation site was positioned just upstream of the surface cyclone and close to the 650-hPa trough, in which the upper-level cyclonic flow increased conditions of inertial stability (Figure 5). The negative value for term (A) ( $-18.6 \cdot 10^{-9} \text{ s}^{-2}$ ) at KMKC confirms the inertial stability. Since term (B1) is always positive ( $4.1 \cdot 10^{-3} \text{ m}^3 \text{ kg}^{-1} \text{ K}^{-1}$ ) and strictly limited to fluctuations in the magnitude of the temperature (K), the other two contributions determine the overall sign for term (B). The moist static stability counterpart represented by (B3) was small ( $-0.4 \cdot 10^{-4} \text{ K m s}^2 \text{ kg}^{-1}$ ) and indicated a

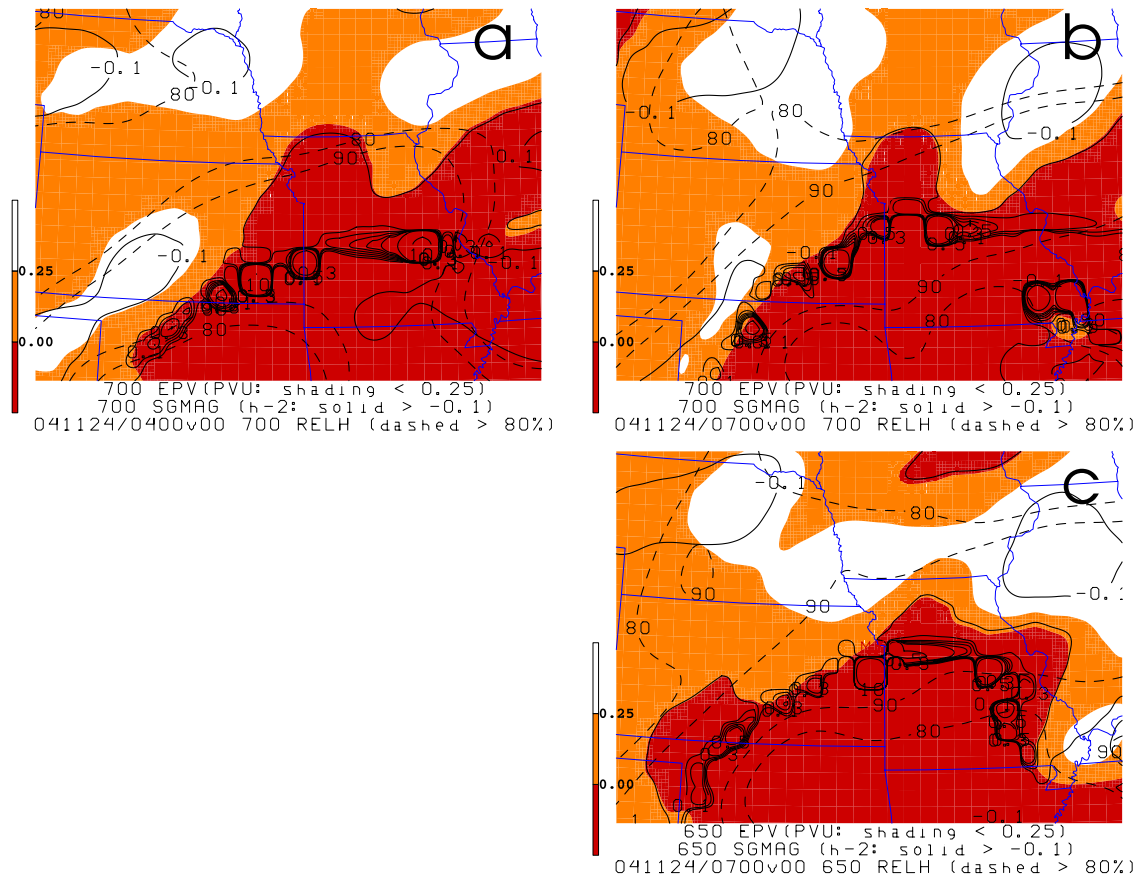


**Figure 6.** Initial analysis of the growth rate parameter ( $\sigma^2$ ;  $h^{-2}$ , solid lines  $> -0.1$ ), 3-D equivalent potential vorticity (EPV;  $10^{-6} \text{ K kg}^{-1} \text{ m}^2 \text{ s}^{-1}$ , color shading  $< 0.25$ ), and relative humidity (dashed for 80% and higher) from the 40-km RUC model. Panels (a) and (b) correspond to the 700-hPa level, with panel (c) corresponding to the LHSGR. The left panel (a) is valid at 0400 UTC 24 November 2004 while the right panels (b, c) are valid at 0700 UTC 24 November 2004. Location of initiation site is represented by surface station identifier MKC (Kansas City, MO).

slight increase with height in the wet-bulb potential temperature for this particular event, with Figure 5 showing regions of gravitational instability farther south in the warmer air, away from where thundersnow began. This of course required the humidity and thermal gradients in the middle troposphere to point in the same direction in order for  $\sigma^2$  to be positive, which occurred here ( $3.2 \cdot 10^{-10} \text{ K}^2 \text{ m}^{-2}$ ; Figure 5) when the warm, moist conveyor belt ascended and intruded into the colder environment north of the surface cyclone. Given an atmosphere not conducive to pure horizontal or vertical displacements, the only other unstable displacement possible is a combination of both in the form of slantwise convection released from CSI.

#### 4.2.3. Cross-Sections

[29] Further confirmation of the stability regime can be obtained by employing other techniques. For the usual  $M_g - \theta_e$  relationship, as described by Snook [1992] and Schultz and Schumacher [1999], a saturated parcel would experience an unstable slantwise path, tilted back toward the colder air, if the displacement is between the  $M_g$  and the more steep  $\theta_e$  surfaces. Following Moore and Lambert [1993], a cross-section is constructed by first identifying the orientation of the baroclinic zone from the 850–300 hPa

thickness field (not shown). Endpoints for the cross-section are subsequently taken across the midtropospheric frontal zone, positioned from southwest to northeast over the Central Plains, such that the area of interest (Kansas City, Missouri) is approximately the midpoint. As a result, values of  $M_g$ ,  $\theta_e$ , and relative humidity greater than 80% are plotted in Figure 7 on an x-z plane extending from Aurora, Nebraska (KAUH) to Fort Leonard Wood, Missouri (KTBN).

[30] Conditions for the occurrence of slantwise convection would be present within the outlined region over and encompassing the initiation site, centered mainly between 600–700 hPa (Figure 7). In this confined location, sufficient baroclinicity was juxtaposed in a nearly saturated and moist neutral atmosphere. By progressing from left to right in the cross-section, significant variations in the across-frontal 3-D dynamical shear and thermodynamic lapse rates are evident as the atmosphere transitions from weak symmetric stability to CI in the relatively warmer air ahead of the frontal boundary (Figure 7). The evaluation is supported further by the shaded values of EPV for the same cross-section (Figure 8). This typical configuration with conditions of CSI present in the middle of the profile compares

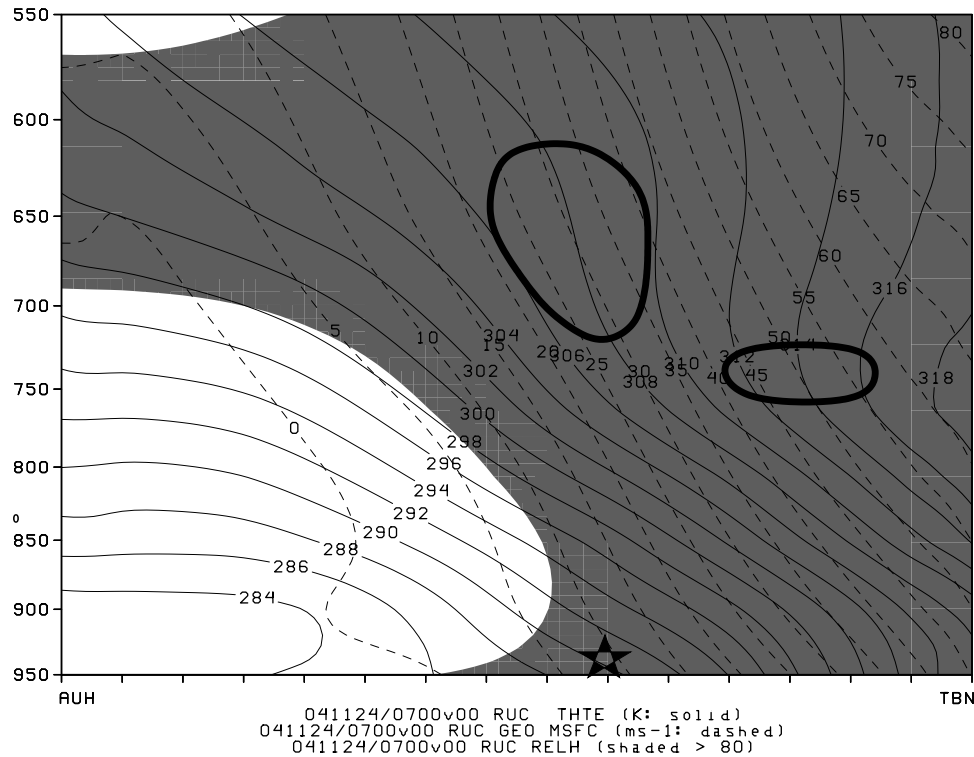


**Figure 7.** 40-km RUC cross-section analysis of geostrophic pseudo-angular momentum ( $M_g$ ;  $\text{m s}^{-1}$ , dashed lines), equivalent potential temperature ( $\theta_e$ ; K, solid lines), and relative humidity greater than 80% (shading) valid at 0700 UTC 24 November 2004. The cross-section extends from Aurora, NE (KAUH) to Fort Leonard Wood, MO (KTBN) with temperatures increasing to the right and the star representing approximate location of Kansas City, MO. Solid black circle highlights atmospheric region deemed susceptible to the release of CSI.

well to the schematic by Jim Moore and Sean Nolan, as formalized by *Schultz and Schumacher* [1999, Figure 4]. Moreover, a complete 3-D inspection reveals that the inclusions of growth rates constrict the most favored region for increased electrical activity to not just a horizontal but a vertical extent as well (Figure 8). The highest positive readings of  $\sigma^2$  are situated between 700–650 hPa (Figure 8) where the lapse rates of  $\theta_e$  are minimal.

[31] As discussed by both *Bennetts and Hoskins* [1979] and *Emanuel* [1983a], the release of CSI within this preferred region will produce slanted roll circulations oriented parallel to the thermal wind. Maximum magnitudes for the enhanced vertical motions can be on the order of a few  $\text{m s}^{-1}$  (something which the RUC-2 could not explicitly resolve), this being marginal in meeting the necessary threshold for the generation of lightning [e.g., *Zipser and Lutz*, 1994; *Schultz and Schumacher*, 1999]. However, the generated circulation would act to overturn the  $\theta_e$  surfaces, if given sufficient time, which would thus indicate strong growth of the instability (compare Figures 7, 8, and 9 with *Emanuel* [1983a, Figure 5]) and an atmosphere more prone to gravitational convection. Should these motions produce conditions of CI, the banded nature of the snowfall would be stronger, with a higher probability of cloud electrical discharges. In addition to the synoptic-scale processes described previously, a mechanism for lifting air parcels to the slantwise level of free convection is apparently provided partly by a sloping zone of geostrophic frontogen-

esis shown in Figure 9. The plan view wind pattern at 650-hPa further reveals that the mesoscale forcing was presumably the result of a deformation zone stretching across northern Missouri into the southeastern part of Kansas (Figure 5). The inferred, moist slantwise convection is supported by an examination of the generated, ageostrophic circulation, such that a slightly tilted pattern is observed with substantial upward vertical velocities ( $12\text{--}16 \mu\text{b s}^{-1}$ ) collocated near the LHSGR (Figures 8 and 9).

## 5. Composites and Comparison to Non-TSSN Events

[32] The composite plots produced here complemented the profile results from a single location. The analyses offered a way to inspect the spatial distribution of stability characteristics and visually track their movement with respect to the most intensive part of the snowstorm (whether or not lightning was present). Averages of  $\sigma^2$  ( $\text{h}^{-2}$ ) and 3-D EPV ( $10^{-6} \text{K kg}^{-1} \text{m}^2 \text{s}^{-1}$ ) were obtained for each grid point in the smaller domain and combined together to refine the forecast area deemed susceptible to convective development. Since the mean pressure level for the LHSGR was not a standard 50-hPa as in a numerical weather model, the closest approximation for both data sets and time periods was determined to be 650-hPa for the composites. The addition of standard deviations gave value ranges for the two stability parameters near the area of interest. Finally,

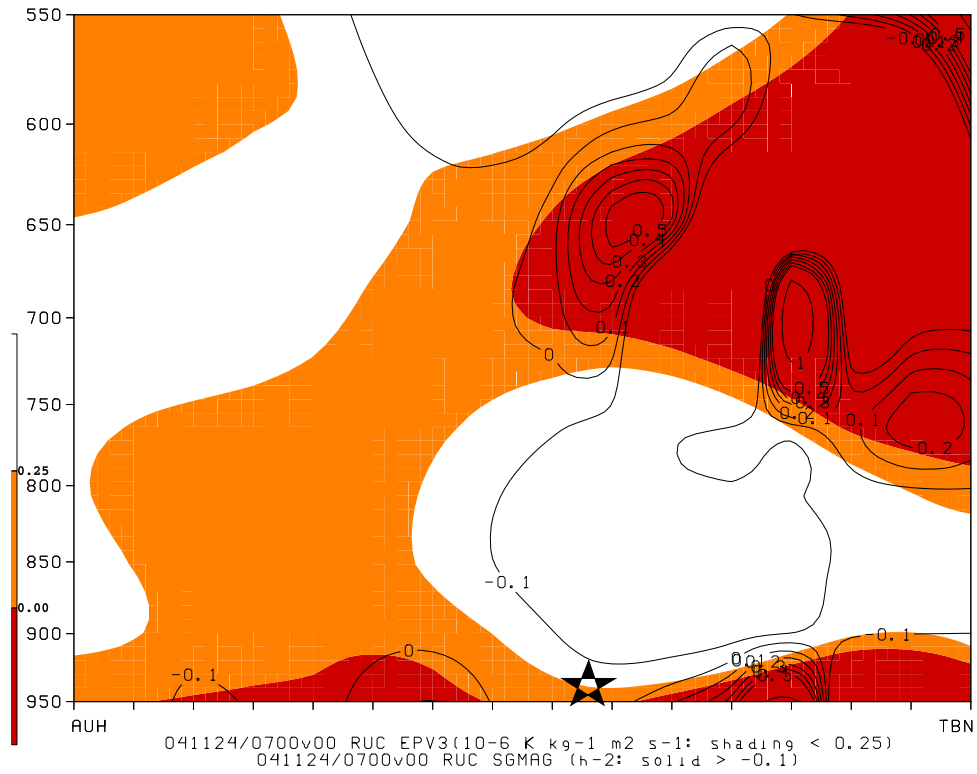


**Figure 8.** As in Figure 7 except for the growth rate parameter ( $\sigma^2$ ;  $h^{-2}$ , solid lines  $> -0.1$ ) and 3-D equivalent potential vorticity (EPV;  $10^{-6} \text{ K kg}^{-1} \text{ m}^2 \text{ s}^{-1}$ , color shading  $< 0.25$ ).

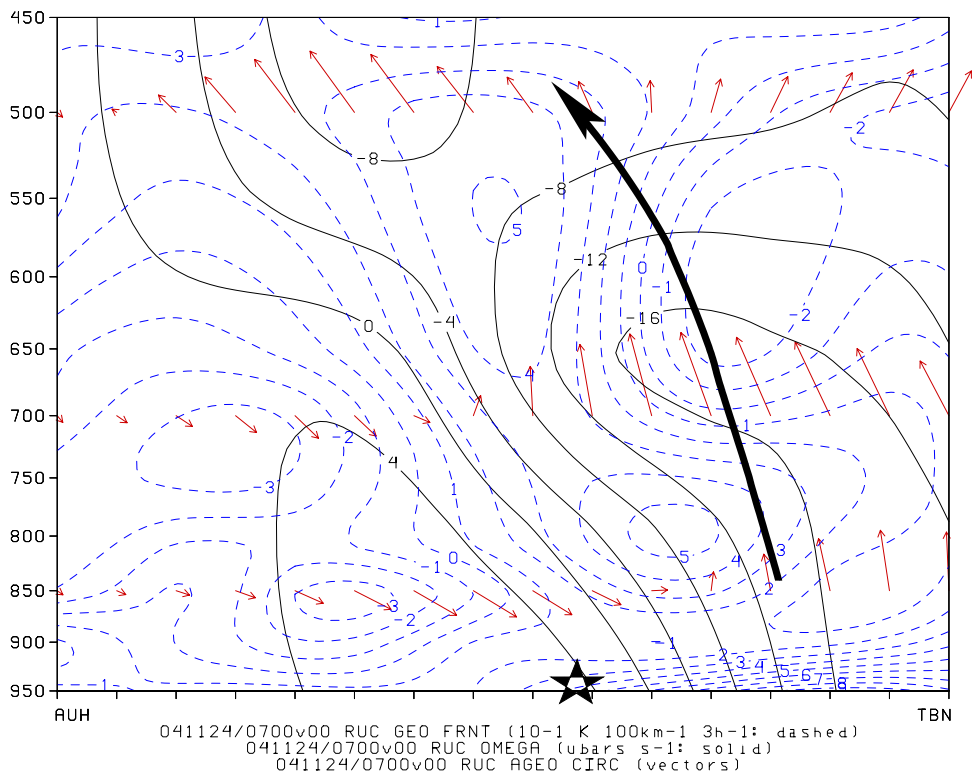


**Figure 9.** As in Figure 7 except for ageostrophic circulation (vectors), isobaric vertical velocity ( $\mu\text{bars s}^{-1}$ , solid lines), and 2D geostrophic frontogenesis ( $\text{K } 100 \text{ km}^{-1} \text{ 3 h}^{-1}$ , dashed lines).

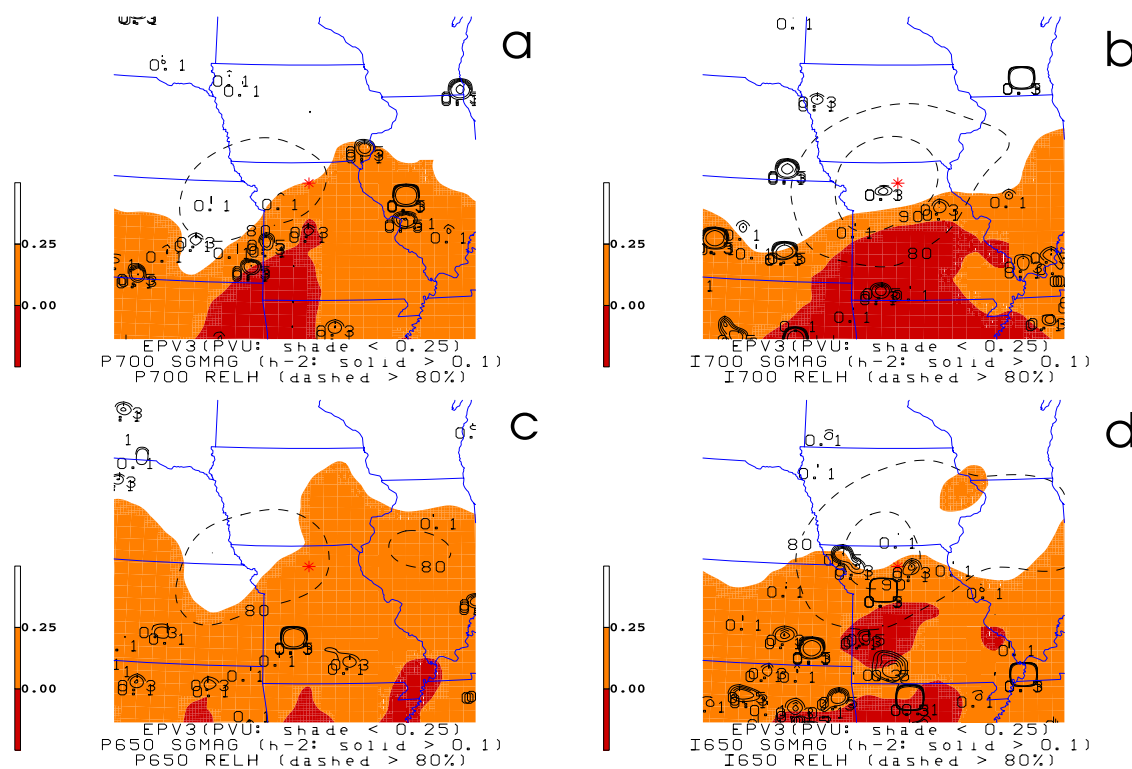


**Figure 10.** Spatial average composites of  $\sigma^2$  ( $\text{h}^{-2}$ ; solid lines  $>0.1$ ), 3-D EPV ( $10^{-6} \text{ K kg}^{-1} \text{ m}^2 \text{ s}^{-1}$ ; orange shading  $<0.25$  and red shading  $<0$ ), and RH (dashed lines for 80% and higher) from the 40-km RUC model. Panels (b) and (d) represent the time of initiation, whereas panels (a) and (c) represent three hours prior. Plots at the 700-hPa level (a, b) and the LHSGR (approx. 650-hPa; c, d) are presented. The background map is utilized as reference only and the asterisk denotes the approximate position for the average (or typical) TSSN initiation site.

the background maps are shown as reference only and, at best, symbolize the representative area of interest for the case studies.

[33] Figure 10 shows  $\sigma^2$ , 3-D EPV, and RH calculated from the RUC-2 model for the set of previously identified convective snow case studies in this study. The smoothed fields show a small area of instability along the southern border (Figures 10a and 10c) that expanded a little northward by the time the first CG-lightning occurs (Figures 10b and 10d). A larger, surrounding region of slightly stable conditions extended farther into the polar air mass and near the TSSN initiation site. This information is revealed by the orange (red) shaded extent of 3-D EPV values of less than 0.25 (less than zero). The release of either CI or CSI was permitted given the collocation of a nearly saturated atmosphere. While there are some variations in the 3-D EPV pattern depending upon time frame or pressure level selected, the contoured plots of growth rates vary much more. Pockets of higher, positive  $\sigma^2$  propagate closer to the centroid over the course of the three hours, with panels (c) and (d) in Figure 10 indicating that the LHSGR exhibited the most favorable increase in values. Consequently, as would be expected, the typical atmosphere near thunderstorm development in winter precipitation events is one that shows signs of destabilization.

[34] The standard deviation plots for TSSN events, shown in Figure 11, revealed that variations in values of both  $\sigma^2$

and 3-D EPV were noticeable among the time periods and pressure levels (700-hPa and LHSGR). The shaded regions of growth rates near the area of interest indicated that the range was on the order of the averages established in Figure 10. However, the greatest concentration of darker shading, cellular features tended to be displaced toward the south. This pronounced signature was most likely the result of the often localized and spotty nature of convectively unstable air masses within the warm sector of synoptic scale disturbances, where lapse rates in  $\theta_w$  (i.e., term B3) tend to be less (and more often approach conditions of neutrality) than locations poleward of the ETC. On the other hand, the standard deviations in 3-D EPV were not as substantial and never approached in the spatial analysis an order of magnitude larger than the associated mean values shown in Figure 10. The trends in the RUC-2 patterns leading up to convective initiation (compare panels b, d to a, c in Figure 11) were somewhat ambiguous, as the assessment depended on the selected parameter and spatial coordinates, which can be prescribed by horizontal distance relative to initiation site as well as vertical placement. This complexity is not surprising with respect to  $\sigma^2$  as the regions of greatest magnitude are present over a very confined domain that can often change in size, orientation, shape, and precise location with respect to initiation site as the synoptic environment naturally evolves from one event to the next. While it is true that the mean fields in the

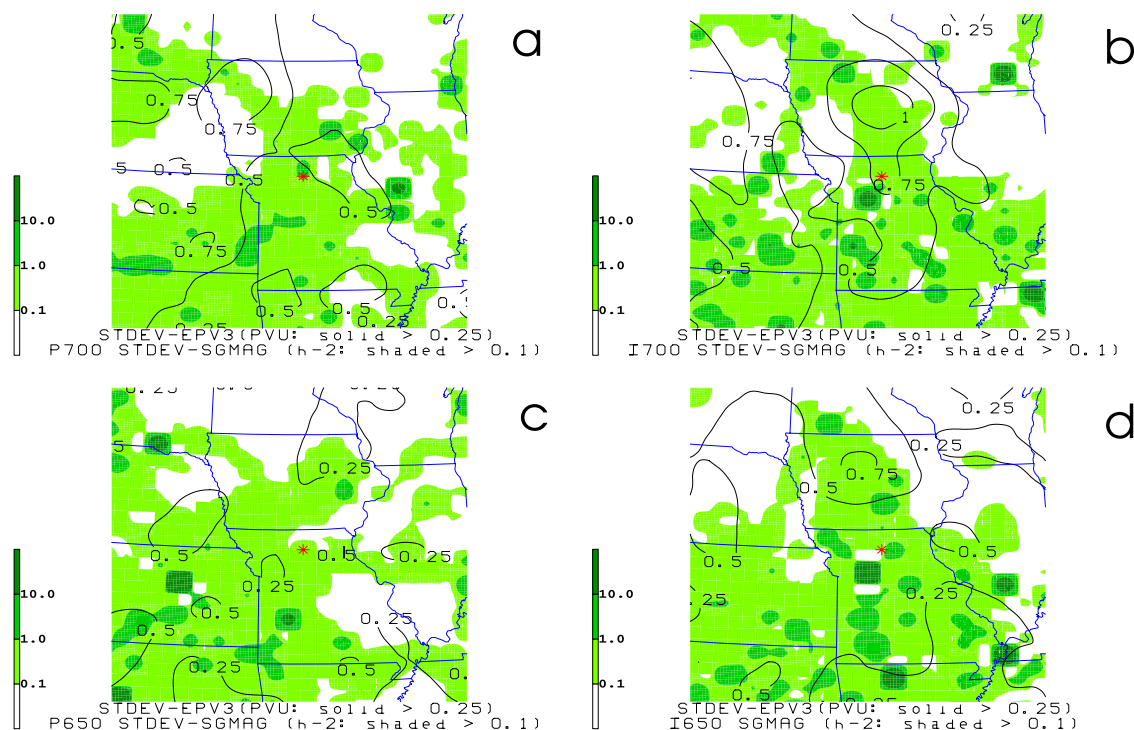


**Figure 11.** Spatial standard deviation composites of  $\sigma^2$  ( $\text{h}^{-2}$ ; green shading  $>0.1$ ) and 3-D EPV ( $10^{-6} \text{ K kg}^{-1} \text{ m}^2 \text{ s}^{-1}$ ; solid lines  $>0.25$ ) from the 40-km RUC model. Panels and background map are same as that in Figure 10.

composites (Figure 10) would be more representative of *all* thundersnow occurrences if the relatively limited number of events collected were expanded, it is speculated that some of the variability prevalent in Figure 11 might be inherent to the unique combination of factors influencing the diagnosis of growth rates in the atmosphere.

[35] Table 5 shows a similar list of parameters but for the alternate group of non-TSSN events. Characteristic results of  $\sigma^2$  (3-D EPV) increased (decreased) over the three hour period ending at the midpoint for both the 700-hPa (Table 5A) and the LHSGR (Table 5B). The latter method was once again associated with relatively reduced stability and elevated growth rates over the former. As was the scenario for TSSN, a large range in values is evident in Table 5 as standard deviations were about on the same order as the averages. Despite this resemblance, the obvious distinction is the larger 3-D EPV and smaller  $\sigma^2$  statistics in winter storms lacking CG-lightning (contrast Tables 4 and 5). In fact, an evaluation of equations (2) and (3) in Table 5B ( $-0.06 \pm 0.11 \text{ h}^{-2}$  and  $0.24 \pm 0.39 \cdot 10^{-6} \text{ K kg}^{-1} \text{ m}^2 \text{ s}^{-1}$ ) versus that of Table 4B ( $0.30 \pm 0.59 \text{ h}^{-2}$  and  $-0.03 \pm 0.25 \cdot 10^{-6} \text{ K kg}^{-1} \text{ m}^2 \text{ s}^{-1}$ ) indicated that the signs for the left-hand-side expressions at the LHSGR and the later time period had a tendency to be opposite to those for TSSN. As a result, the correlation between the two data sets advanced some evidence that instability and destabilization of the environment was more prevalent for instances of cold-season moist convection.

[36] The similarity in synoptic-scale features (e.g., transient ETC) for both sets of snowstorms meant that the necessary dynamic and thermodynamic forcing mechanisms are present in either case (not shown). In order to effectively

identify discrepancies, other ingredient factors for thunderstorm development must be considered. For this purpose, composites of non-TSSN events are displayed in Figure 12. Zones of  $\sigma^2$  greater than zero were displaced farther equatorward compared to Figure 10, with the lower 3D-EPV estimates not as evident within the domain. Although high RH values near the midpoint site suggest an atmosphere saturated enough for the production of precipitation, these plots indicate the stability regime was insufficient for the development of moist convection in the snowstorm (Figure 12). The smaller number of case studies utilized in the identification process compared to its counterpart would often lead one to conclude that the spatial distribution of standard deviations are greater. An inspection of the statistics in Figure 13 against those in Figure 11 corroborates this assumption at least for 3-D EPV in and around the area of interest. In fact, the continuity in the contoured field was more discernible and made tracking the progression and intensification of the maxima for this stability diagnostic much easier. As for  $\sigma^2$ , however, the variations in all time

**Table 5.** Same as in Table 4 Except for Non-TSSN Events, With Calculations Valid at the Midpoint Location and Time Period as Well as 3-Hours Prior

(A) 700-hPa	Midpoint	Prior
$\sigma^2$	-0.11 (0.11)	-0.13 (0.09)
3-D EPV	0.72 (0.71)	0.84 (0.61)
(B) LHSGR(hPa)	Midpoint	Prior
$\sigma^2$	-0.06 (0.11)	-0.08 (0.11)
3-D EPV	0.24 (0.39)	0.53 (0.58)

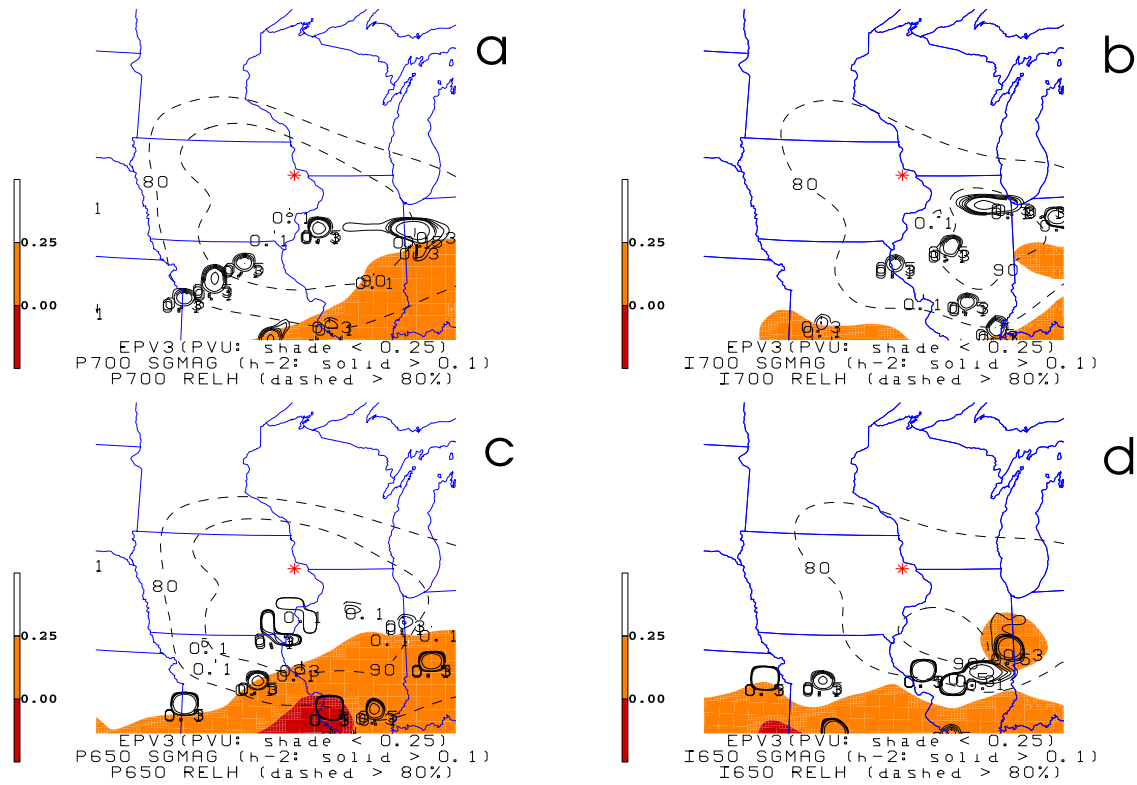


**Figure 12.** Same as in Figure 10 except for non-TSSN events compiled. The asterisk denotes the approximate position for the average (or typical) non-TSSN midpoint site.

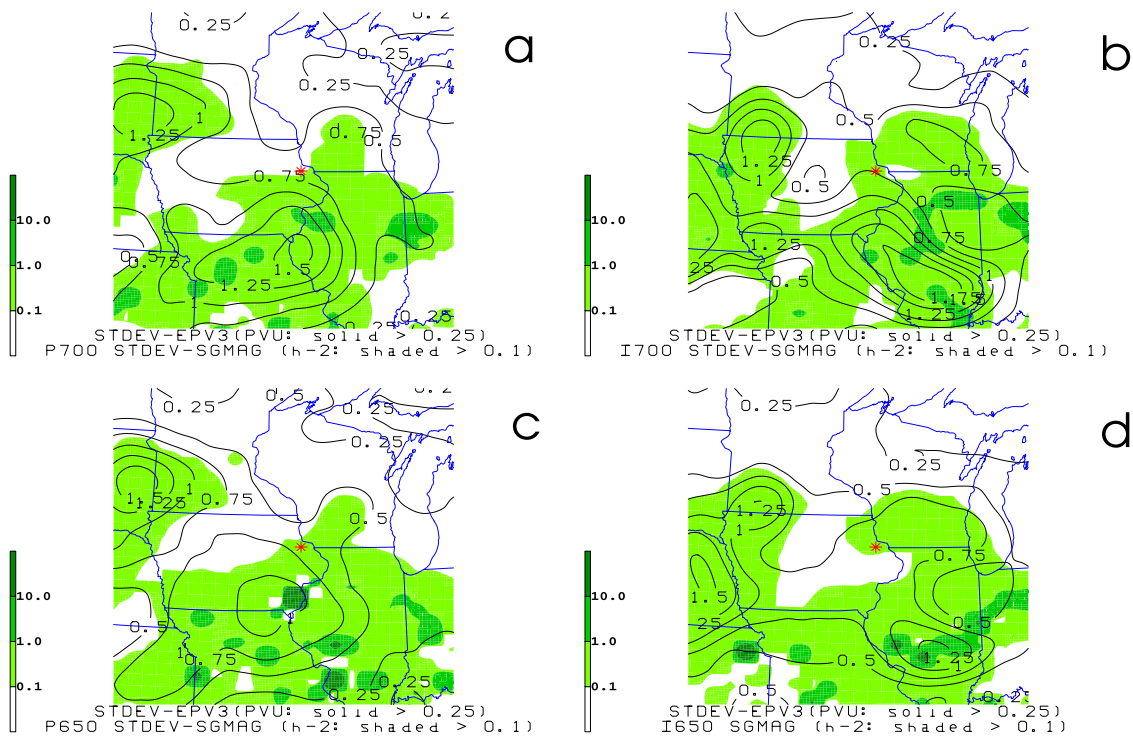


**Figure 13.** Same as in Figure 11 except for non-TSSN events compiled.

frames and elevations (Figure 13) were diminished overall throughout the domain. This is to be expected since the constituent environment of non-TSSN events is generally colder compared to those snowstorms that feature lightning [e.g., see *Market et al.*, 2006, Figure 3] and, thus should be displaced farther away from an atmosphere prone to upright or slantwise displacements in almost all instances.

## 6. Conclusions

[37] Throughout the current investigation, the main goal was to make a detailed examination of  $\sigma^2$  and corroborate the initial findings by *Bennetts and Sharp* [1982], while providing additional insights into stability characteristics associated with wintertime, elevated thunderstorms. This is accomplished by utilizing two seasons (2003–2004 and 2004–2005) worth of data and including a separate group of non-TSSN episodes in the study to stress the findings about  $\sigma^2$ . Unlike *Bennetts and Sharp* [1982], however, the lower number of events available to examine here demand caution and permit formulation of only broad guidelines for operational use. Upon comparison against the observational evidence (surface weather observations, NLDN, radar reflectivity), this work showed that, on average,  $\sigma^2$  was very useful in accurately anticipating that the atmospheric environment was destabilizing immediately leading up to the onset of convection. Through both tabular and graphical (case study and composites) means, greater success was found in obtaining estimates at the LHSGR. This selection was physically more reasonable compared to restricting the analysis to one level in all the thundersnow events since a more ideal situation for convective development is usually where the least resistance to convection is observed. While the existence of precipitation bands tended to become more likely with higher, positive growth rates ( $\sigma^2 > 0.2 \text{ h}^{-2}$ ), that value alone was insufficient for discriminating the type of convective structures to expect. Proper awareness of the development of possible mesoscale precipitation bands required recognizing shapes in the 2-D analyses of  $\sigma^2$ , an objective not possible with single interpolated estimates. Determining whether the anticipated convective, vertical circulations took on more of an upright or slantwise nature was permitted by performing a term-by-term diagnosis of equation (2). This methodology proved to be another valuable approach to establishing the kind of stability regime present.

[38] The case study example provided a practical glimpse into the 3-D spatial distributions of stability characteristics and their evolution with time. The presence of abundant moisture, ample forcing for perturbing air parcels upward, and the enhancement of those vertical motions from symmetric instability in this case were responsible for the occurrence of thundersnow. In addition, the numerous CG lightning flashes observed near the time of initiation were supported by a continued downward trend in the stability regime via positive growth rates. As for the other instances of convective snowfall, the relatively high values for the standard deviation for both  $\sigma^2$  and EPV in Table 4 would tend to indicate large differences in conditions for the small sample size. Still, negative (positive) values of the former (latter) parameter occurred at initiation only five times when evaluated from the LHSGR (not shown). In addition, the

corresponding magnitudes were often small, thereby keeping resistance to convection at a minimum. The other ingredients for thunderstorms, a nearly saturated environment and robust dynamics to produce updrafts, were present in all events. Given the repeated correlations and similarities noted from the current investigation, the usefulness of  $\sigma^2$  could be more thoroughly measured by comparing plots of the prognostic parameter against plan view radar analyses as well as other observational networks.

[39] Composite of  $\sigma^2$  and 3-D EPV were also produced since a lone case study is not capable of providing conclusive evidence on the summary of typical stability features present in and around the area where the first TSSN report occurs. Although not identical to the event relied upon in this study, the averaged fields were similar in many respects and complemented each other effectively in the final analysis. Moreover, the plots of standard deviations were presumably characteristic to the sample size available and the nature of the stability parameters examined. Along with the tabular statistics discussed, the main conclusion reached here follows that of *Market et al.* [2006], in which the diagnostics imply an environment less resistant to upward motions in occurrences of TSSN compared to an otherwise comparable collection of non-TSSN events. As a result, the utility of  $\sigma^2$  in discriminating the time and place of convection in snowstorms was bolstered by applying the multiple, comprehensive approaches in the current investigation.

[40] Some of the techniques employed by this work could be useful for routine implementation in an operational environment. Since episodes of convective snowfall often produce intense rates of precipitation over a concise time period and small spatial scale, which can often result in hazardous traveling conditions, more precise and accurate means of anticipating significant wintertime weather events are always needed by forecasters. Similar to what was recommended by *Bennetts and Sharp* [1982],  $\sigma^2$  and its terms could be computed easily using simple scripts with output generated from fine resolution models. Further, by combining the growth rates with other measures of stability (such as EPV), the areal extent and temporal duration of potential elevated convection could be narrowed down. This would hopefully provide another tool to help forecasters in predicting the likelihood of banded precipitation and determining the type of instability present.

[41] **Acknowledgments.** Rapid Update Cycle data were obtained from the Atmospheric Radiation Measurement (ARM) Program sponsored by the U.S. Department of Energy, Office of Science, Office of Biological and Environmental Research, Environmental Sciences Division. The paper presented here is part of the doctoral work that the primary author is completing while at the University of Missouri-Columbia. This work is supported by the National Science Foundation (NSF), Award No. ATM-0239010. Any opinions, findings, conclusions or recommendations expressed herein are those of the author(s) and do not necessarily reflect the views of NSF.

## References

- Barnes, S. L., F. Caracena, and A. Marroquin (1996), Extracting synoptic-scale diagnostic information from mesoscale models: The Eta model, gravity waves, and quasigeostrophic diagnostics, *Bull. Am. Meteorol. Soc.*, 77, 519–528.
- Benjamin, S. G., J. M. Brown, K. J. Brundage, B. E. Schwartz, T. G. Smirnova, T. L. Smith, and L. L. Morone (1998), RUC-2- The rapid update cycle version 2. NWS technical procedures bulletin no. 448, *NOAA/NWS*, 18 pp. [Available online at: <http://maps.fsl.noaa.gov/ruc2.tpb.html>].

- Benjamin, S. G., G. A. Grell, J. M. Brown, T. G. Smirnova, and R. Bleck (2004a), Mesoscale weather prediction with the RUC hybrid isentropic-terrain-following coordinate model, *Mon. Weather Rev.*, *132*, 473–494.
- Benjamin, S. G., et al. (2004b), An hourly assimilation-forecast cycle: The RUC, *Mon. Weather Rev.*, *132*, 495–518.
- Bennetts, D. A., and B. J. Hoskins (1979), Conditional symmetric instability – A possible explanation for frontal rainbands, *Q. J. R. Meteorol. Soc.*, *105*, 945–962.
- Bennetts, D. A., and J. C. Sharp (1982), The relevance of conditional symmetric instability to the prediction of mesoscale frontal rainbands, *Q. J. R. Meteorol. Soc.*, *108*, 595–602.
- Bjerknes, J., and H. Solberg (1922), Life cycle of cyclones and the polar front theory of atmospheric circulation, *Geofis. Publ.*, *3*, 1–18.
- Browning, K. A. (1990), Organization of clouds and precipitation in extratropical cyclones, in *Extratropical Cyclones, The Erik Palmén Memorial Volume*, edited by C. W. Newton and E. O. Holopainen, pp. 129–153, Am. Meteorol. Soc., Boston, MA.
- Byrd, G. P. (1989), A composite analysis of winter season overrunning precipitation bands over the Southern Plains of the United States, *J. Atmos. Sci.*, *46*, 1119–1132.
- Carlson, T. N. (1980), Airflow through midlatitude cyclones and the comma cloud pattern, *Mon. Weather Rev.*, *108*, 1498–1509.
- Clark, J. H. E., R. P. James, and R. H. Grumm (2002), A reexamination of the mechanisms responsible for banded precipitation, *Mon. Weather Rev.*, *130*, 3074–3086.
- Crowe, C., P. S. Market, B. Pettegrew, C. Melick, and J. Podzimek (2006), An investigation of thundersnow and deep snow accumulations, *Geophys. Res. Lett.*, *33*, L24812, doi:10.1029/2006GL028214.
- Curran, J. T., and A. D. Pearson (1971), Proximity soundings for thunderstorms with snow, paper presented at 7th Conference on Severe Local Storms, Am. Meteorol. Soc., Kansas City, MO.
- desJardins, M. L., K. F. Brill, and S. S. Schotz (1991), Use of GEMPAK on Unix workstations, paper presented at 7th International Conference on Interactive Information and Processing Systems for Meteorology, Oceanography, and Hydrology, Am. Meteorol. Soc., New Orleans, LA.
- Emanuel, K. A. (1983a), The Lagrangian parcel dynamics of moist symmetric instability, *J. Atmos. Sci.*, *40*, 2368–2376.
- Emanuel, K. A. (1983b), On assessing local conditional symmetric instability from atmospheric soundings, *Mon. Weather Rev.*, *111*, 2016–2033.
- Emanuel, K. A. (1986), Overview and definition of mesoscale meteorology, in *Mesoscale Meteorology and Forecasting*, edited by P. S. Ray, pp. 1–17, Am. Meteorol. Soc., Boston, MA.
- Hane, C. E. (1986), Extratropical squall lines and rainbands, in *Mesoscale Meteorology and Forecasting*, edited by P. S. Ray, pp. 359–389, Am. Meteorol. Soc., Boston, MA.
- Holle, R. L., and J. V. Cortinas (1998), Thunderstorms observed at surface temperatures near and below freezing across North America, paper presented at 19th Conference on Severe Local Storms, Am. Meteorol. Soc., Minneapolis, MN.
- Houze, R. A., Jr., P. V. Hobbs, K. R. Biswas, and W. M. Davis (1976), Mesoscale rainbands in extratropical cyclones, *Mon. Weather Rev.*, *104*, 868–878.
- Johns, R. J., and C. A. Doswell III (1992), Severe local storms forecasting, *Weather Forecasting*, *7*, 588–612.
- Jurewicz, M. L., and M. S. Evans (2004), A comparison of two banded, heavy snowstorms with very different synoptic settings, *Weather Forecasting*, *19*, 1011–1028.
- Market, P. S., C. E. Halcomb, and R. L. Ebert (2002), A climatology of thundersnow events over the contiguous United States, *Weather Forecasting*, *17*, 1290–1295.
- Market, P. S., A. M. Oravetz, D. Gaede, E. Bookbinder, R. Ebert, and C. Melick (2004), Upper air constant pressure composites of midwestern thundersnow events, paper presented at 20th Conference on Weather Analysis and Forecasting, Am. Meteorol. Soc., Seattle, WA.
- Market, P. S., et al. (2006), Proximity soundings of thundersnow in the central United States, *J. Geophys. Res.*, *111*, D19208, doi:10.1029/2006JD007061.
- Martin, J. E. (1998), The structure and evolution of a continental winter cyclone. Part II: Frontal forcing of an extreme snow event, *Mon. Weather Rev.*, *126*, 329–348.
- McCann, D. W. (1995), Three-dimensional computations of equivalent potential vorticity, *Weather Forecasting*, *10*, 798–802.
- Moore, J. T., and T. E. Lambert (1993), The use of equivalent potential vorticity to diagnose regions of conditional symmetric instability, *Weather Forecasting*, *8*, 301–308.
- Moore, J. T., F. H. Glass, C. E. Graves, S. M. Rochette, and M. J. Singer (2003), The environment of warm-season elevated thunderstorms associated with heavy rainfall over the central United States, *Weather Forecasting*, *18*, 861–878.
- Moore, J. T., C. E. Graves, S. Ng, and J. L. Smith (2005), A process oriented methodology toward understanding the organization of an extensive mesoscale snowband: A diagnostic case study of 4–5 December 1999, *Weather Forecasting*, *20*, 35–50.
- Mote, T. L., D. W. Gamble, S. J. Underwood, and M. L. Bentley (1997), Synoptic-scale features common to heavy snowstorms in the southeast United States, *Weather Forecasting*, *12*, 5–23.
- Nicosia, D. J., and R. H. Grumm (1999), Mesoscale band formation in three major northeastern United States snowstorms, *Weather Forecasting*, *14*, 346–368.
- Novak, D. R., L. F. Bosart, D. Keyser, and J. S. Waldstreicher (2004), An observational study of cold season-banded precipitation in Northeast U.S. cyclones, *Weather Forecasting*, *19*, 993–1010.
- Oravetz, A. M. (2003), Composite analysis of thundersnow events in the central United States, M. S. Thesis, Department of Atmospheric Sciences, University of Missouri-Columbia, Columbia, MO.
- Parsons, D. B., and P. V. Hobbs (1983), The mesoscale and microscale structure and organization of clouds and precipitation in midlatitude cyclones. XI: Comparisons between observational and theoretical aspects of rainbands, *J. Atmos. Sci.*, *40*, 2377–2397.
- Sanders, F., and L. F. Bosart (1985), Mesoscale structure in the megalopolitan snowstorm of 11–12 February 1983. Part I: Frontogenetical forcing and symmetric instability, *J. Atmos. Sci.*, *42*, 1050–1061.
- Schultz, D. M. (1999), Lake-effect snowstorms in northern Utah and western New York with and without lightning, *Weather Forecasting*, *14*, 1023–1031.
- Schultz, D. M., and P. N. Schumacher (1999), The use and misuse of conditional symmetric instability, *Mon. Weather Rev.*, *127*, 2709–2732.
- Smith, L. L. (2006), Investigating stability evolution of snow storms featuring lightning, M.S. Thesis, Department of Soil, Environmental, and Atmospheric Sciences, University of Missouri-Columbia, 136 pp. (Available online at: <http://solberg.snr.missouri.edu/ROCS/pub/Smith-thesis.pdf>).
- Smith, L. L., C. J. Melick, and P. S. Market (2005), Examination of thundersnow cases in the United States utilizing NLDN data, paper presented at Conference on Meteorological Applications of Lightning Data, Am. Meteorol. Soc., San Diego, CA.
- Snook, J. S. (1992), Current techniques for real-time evaluation of conditional symmetric instability, *Weather Forecasting*, *7*, 430–439.
- Wallace, J. M., and P. V. Hobbs (1977), *Atmospheric Science: An Introductory Survey*, 467 pp., Academic Press, San Diego, CA.
- Weismuller, J. L., and S. M. Zubrick (1998), Evaluation and application of conditional symmetric instability, equivalent potential vorticity, and frontogenetic forcing in an operational forecast environment, *Weather Forecasting*, *13*, 84–101.
- Wetzel, S. W., and J. E. Martin (2001), An operational ingredients-based methodology for forecasting mid-latitude winter season precipitation, *Weather Forecasting*, *16*, 156–167.
- Zipser, E. J., and K. R. Lutz (1994), The vertical profile of radar reflectivity of convective cells: A strong indicator of storm intensity and lightning probability?, *Mon. Weather Rev.*, *122*, 1751–1759.

A. E. Becker, A. R. Lupo, P. S. Market, C. J. Melick, and B. P. Pettegrew, Department of Soil, Environmental and Atmospheric Sciences, University of Missouri-Columbia, 302 ABNR Building, Columbia, MO 65211, USA. (marketp@missouri.edu; cjmzr5@mizzou.edu)

L. L. Smith, National Weather Service, Monterey, CA, USA. (larry.smith@noaa.gov)